Analyst

PAPER

View Article Online
View Journal | View Issue

Cite this: *Analyst*, 2015, **140**, 7209

^{19}F NMR-, ESR-, and vis-NIR-spectroelectrochemical study of the unconventional reduction behaviour of a perfluoroalkylated fullerene: dimerization of the $C_{70}(CF_3)_{10}^-$ radical anion†

Michal Zalibera,*[a,b,c] Peter Machata,[a,d] Tyler T. Clikeman,[e] Marco Rosenkranz,[a] Steven H. Strauss,*[e] Olga V. Boltalina*[e] and Alexey A. Popov*[a]

Received 4th June 2015,
Accepted 21st August 2015

DOI: 10.1039/c5an01129a

www.rsc.org/analyst

The most abundant isomer of $C_{70}(CF_3)_{10}$ (**70-10-1**) is a rare example of a perfluoroalkylated fullerene exhibiting electrochemically irreversible reduction. We show that electrochemical reversibility at the first reduction step is achieved at scan rates higher than 500 V s^{-1}. Applying ESR-, vis-NIR-, and ^{19}F NMR-spectroelectrochemistry, as well as mass spectrometry and DFT calculations, we show that the (**70-10-1**)$^-$ radical monoanion is in equilibrium with a singly-bonded diamagnetic dimeric dianion. This study is the first example of ^{19}F NMR spectroelectrochemistry, which promises to be an important method for the elucidation of redox mechanisms of fluoroorganic compounds. Additionally, we demonstrate the importance of combining different spectroelectrochemical methods and quantitative analysis of the transferred charge and spin numbers in the determination of the redox mechanism.

Introduction

Since its early stages and until now, the field of molecular organic semiconductors has had a pronounced imbalance towards p-type materials. Hence, many efforts have been dedicated to the development of n-type organic semiconductors which might be comparable in stability and device performance with their p-type counterparts.[1–5] Functionalization with electron-withdrawing groups, such as F atoms or perfluoralkyl radicals, is one of the common methods used to increase the electron affinity of organic semiconductors and improve the n-type properties of organic semiconductors. For instance, in a series of recent perfluoroalkyl derivatization studies of different polyaromatic hydrocarbons (PAHs) it was shown that each R_F group increases the electron affinity by 0.2–0.3 eV and induces similarly high positive shifts of the electrochemical reduction potentials.[6–14] Hence, poly(perfluoroalkylation) is a convenient way to create strong electron acceptors from virtually any PAH. Likewise, fluorination and perfluoroalkylation of fullerenes has created a range of compounds with enhanced electron-accepting properties.[15–17] For fullerenes, however, the influence of added groups on the electron accepting properties is more complex and strongly depends on the addition pattern.[18]

Electrochemistry is a common tool used to characterize the electron-accepting properties of molecular organic materials. Firstly, the electrochemical reduction potential provides a convenient and simple estimation of the LUMO energy. Secondly, the stability of anion radicals is an important issue for n-type materials, which the electrochemical reversibility of the first reduction step may give preliminary information about. The electrochemical irreversibility of the reduction does not automatically translate to the performance of the materials in the solid state, where the timescale of electron transport is much faster than the typical timescale of cyclic voltammetry measurements. Still, observation of the electrochemically irreversible reduction process raises questions about the possible mechanism of the sample degradation or may be an indication of slow electron transfer kinetics. For instance, fluorofullerenes usually exhibit irreversible reduction behaviour presumably due to the loss of fluorine upon reduction. At the same time, the majority of perfluoroalkylfullerenes have reversible reduction steps,[18,19] although several compounds with irreversible reductions are also known, including the major isomer of

[a]*Leibniz Institute for Solid State and Materials Research, 01069 Dresden, Germany. E-mail: a.popov@ifw-dresden.de*
[b]*Institute of Physical and Theoretical Chemistry, Graz University of Technology, 8010 Graz, Austria*
[c]*Max Planck Institute for Chemical Energy Conversion, 45470 Mülheim and der Ruhr, Germany*
[d]*Institute of Physical Chemistry and Chemical Physics, Faculty of Chemical and Food Technology, Slovak University of Technology, SK-812 37 Bratislava, Slovak Republic*
[e]*Department of Chemistry, Colorado State University, Fort Collins, Colorado 80523, USA*

† Electronic supplementary information (ESI) available: Additional electrochemical and spectroscopic results, mass spectrometry study, and DFT-optimized Cartesian coordinates. See DOI: 10.1039/c5an01129a

$C_{70}(CF_3)_{10}$, which is the main subject of this work. A large fraction of perfluoroalkylated PAHs also exhibits electrochemically irreversible reduction behaviour at moderate voltammetric scan rates.[7,11,14]

Elucidation of the mechanism of complex redox reactions often requires the use of complementary spectroscopic techniques. Spectroelectrochemistry, the combination of spectroscopy and electrochemistry, plays a prominent role in such investigations. A plethora of spectroscopic approaches have been successfully implemented for *in situ* spectroelectrochemical (SEC) studies.[20,21] One of the advantages of SEC is the possibility to address the molecular structures of the species formed during the electron transfer and follow-up chemical reactions. With this goal in mind, a wealth of structural information would be one of the most important requirements for a spectroscopic technique to be used as a SEC tool. Despite the dominant role of NMR spectroscopy in the structural characterization of organic compounds, the coupling of NMR with electrochemistry is used relatively rarely. Fewer than 15 NMR-SEC studies have been published to date.[22–36] The majority utilized ^{1}H NMR-SEC; two papers reported ^{13}C NMR-SEC,[32,33] and NMR with other nuclei has not been applied to our knowledge. In this work we establish, for the first time, ^{19}F NMR-SEC as a powerful tool for the study of the redox mechanisms of fluorinated organic compounds. This method compliments already well established UV-vis-NIR and ESR spectroelectrochemical techniques and is especially useful when the reduction process and/or follow-up reactions produce diamagnetic species. As a working example, we have applied this new tool, along with vis-NIR- and ESR-SEC, to study the reduction/reoxidation behaviour of 1,4,10,19,25,41,49,60,66,69-$C_{70}(CF_3)_{10}$ (Fig. 1, hereafter **70-10-1**). **70-10-1** is the major isomer of $C_{70}(CF_3)_{10}$ and can be obtained with unprecedentedly high yield, thus making it one of the most abundantly produced perfluoroalkylfullerenes. But unlike the majority of other perfluoroalkylfullerenes, which exhibit reversible chemical and electrochemical reduction with the formation of stable radical anions,[18,19,37–40] **70-10-1** was found to have an irreversible reduction with an as yet unknown mechanism.[19] Here we show that the application of our new ^{19}F NMR-SEC approach is crucial to elucidate the reduction mechanism of **70-10-1** and prove that the reversible dimerization of the radical anion is the most plausible explanation.

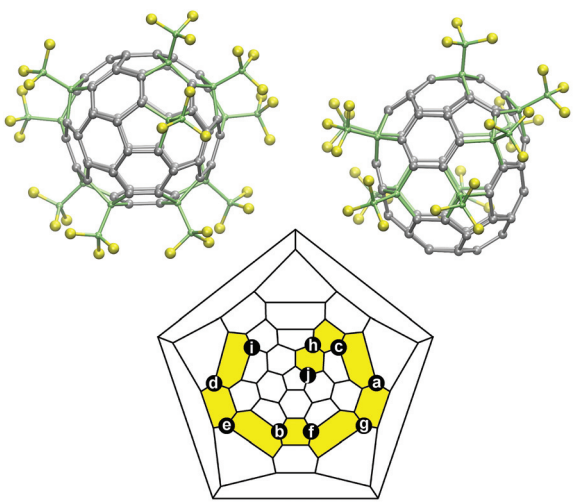

Fig. 1 Molecular structure (two projections) and Schlegel diagram of **70-10-1**. In the molecular structure, fluorine is shown yellow, and carbon is either light green (C-sp^3) or grey (C-sp^2). In the Schlegel diagram, the positions of the CF_3 groups are denoted with black dots, and the white letters correspond to multiplets in the ^{19}F NMR spectrum. The ribbon of edge-sharing *para* or *meta* $C_6(CF_3)_2$ hexagons, formed by 10 CF_3 groups, is highlighted in yellow.

Experimental and computational details

The synthesis of **70-10-1** was previously described.[41]

Fast scan cyclic voltammetry measurements were performed using an Autolab PGSTAT100 potentiostat (Metrohm Autolab, The Netherlands) and a two-electrode cell with a home-made working microelectrode (a Pt wire fused into a glass support, Ø 60 ± 10 μm) and a Pt wire as a counter/reference electrode. The electrolyte solution was 0.1 M tetrabutylammonium tetrafluoroborate ($TBABF_4$) in *o*-dichlorobenzene (*o*-DCB).

In situ ESR/vis-NIR spectroelectrochemical measurements were performed in a Bruker ER 4104OR optical ESR cavity. ESR spectra were recorded using a Bruker EMX Micro X-band CW spectrometer. Vis-NIR spectra were recorded using an Avantes AvaSpec-2048x14-USB2 spectrometer with a CCD detector and an Avantes AvaSpec-NIR256-2.2 spectrometer with an InGaAs detector and AvaSoft 7.5 software. Both the ESR spectrometer and the UV-vis-NIR spectrometers were linked to a HEKA PG 390 potentiostat. Triggering was performed using the software package PotMaster v2x40 (HEKA Electronic). A spectroelectrochemical flat cell with a three-electrode arrangement consisting of a laminated Pt-mesh working electrode, a platinum wire auxiliary electrode, and a silver wire pseudoreference electrode was used.[42] The cell was filled and prepared in an oxygen-free glovebox and was subsequently sealed and transferred to the spectrometers.

The NMR spectroelectrochemical measurements were performed using a Bruker Avance II 500 MHz spectrometer equipped with a standard 5 mm BBO probe head, a BC-U05 heating system, and the software package TopSpin 2.1 (Bruker Biospin). The ^{1}H probe head channel was tuned to 470.6 MHz to run the ^{19}F experiments. Electrochemical experiments were carried out using a three electrode system, a HEKA potentiostat PG 390, and the software package Potmaster (HEKA Elektronik).

The electrode construction consisted of a carbon fiber filament for the working and auxiliary electrodes.[23] Additionally, a thin chlorinated silver wire was located close to the working electrode as a quasi-reference electrode. To study the electrolysis products at the working electrode, only this part of the cell

system was located in the range of the RF coils in the NMR probe. The electrodes were connected to the potentiostat with Cu wires. To house the carbon-fiber-filament working and auxiliary electrodes, glass capillaries were sealed at one end with epoxy resin and wrapped at the other end with PTFE tape. The contact between the carbon fiber and the copper wire was made with conductive epoxy resin. The PTFE-covered chlorinated Ag wire pseudoreference electrode was soldered to a Cu wire and arranged together with the other connecting wires of the working and counter electrode. The electrode system consisting of all three electrodes was inserted into a 5 mm NMR tube and sealed with PTFE tape.

For the *in situ* NMR spectroelectrochemical experiment, *ca.* 2.4 mg of **70-10-1** was dissolved in 0.5 mL of *o*-DCB-d_4 containing 0.3 M $NBu_4^+ClO_4^-$ as the supporting electrolyte, purged with N_2 for 10 min, and transferred to a standard 5 mm NMR tube in an inert-atmosphere glovebox (O_2 and H_2O vapor <1 ppm). A small crystal of $NBu_4^+BF_4^-$ was added as the NMR chemical shift standard. For the chemical reduction, *ca.* 1.4 mg of **70-10-1** was dissolved in 0.5 mL of *o*-DCB-d_4 and titrated with a saturated solution of $CoCp_2$. A few small crystals of $NBu_4^+PF_6^-$ were added to the sample prior to reduction as an internal standard for quantification. All sample-handling operations were performed in the glovebox (O_2, H_2O vapor <1 ppm) and the spectra were recorded in a sealed 5 mm NMR tube.

Selected NMR spectra were also recorded using a Varian Inova 400 instrument (CD_2Cl_2, 376.5 MHz, 298 K, C_6F_6 int. std. (δ −164.9)). Negative-ion atmospheric-pressure chemical ionization (NI-APCI) mass spectra were recorded using an Agilent Technologies Model 6210 TOF spectrometer. Dichloromethane solutions were initially injected and the mobile phase was acetonitrile.

All structures were first optimized at the PBE/TZ2P level using the Priroda code.[43,44] Then, single point energy calculations at the B3LYP-D3/6-311G* level with dispersion correction[45] and the C-PCM[46] solvation model were computed using the Firefly code.[47]

Results and discussion

Cyclic voltammetry

Fig. 2 shows the cyclic voltammograms (CVs) of **70-10-1** in *o*-dichlorobenzene (*o*-DCB) recorded at scan rates of 5 mV s^{-1} and 500 V s^{-1}. The reduction of **70-10-1** is electrochemically irreversible at the lower scan rate (and at scan rates up to 20 V s^{-1} (ref. 19)). Namely, a single reduction peak at −0.11 V *vs.* $C_{70}^{0/-}$ in the forward scan is followed by two re-oxidation peaks near −0.05 V and +0.70 V in the reverse scan (note that the reduction potential for the $C_{70}^{0/-}$ couple is −1.08 V *vs.* $Fe(Cp)_2^{+/0}$ in *o*-DCB). The first re-oxidation peak corresponds to the reversible oxidation of **70-10-1**$^-$ and is insignificant relative to the second re-oxidation peak at 5 mV s^{-1}, and is still less intense than the second re-oxidation peak at scan rates lower than 20 V s^{-1}.[19] Electrochemical reversibility of the first

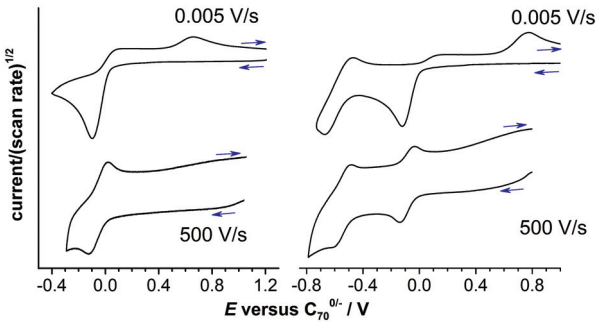

Fig. 2 Cyclic voltammograms of **70-10-1** in *o*-DCB at slow (5 mV s^{-1}) and fast (500 V s^{-1}) scan rates. Arrows show the direction of the scan.

reduction of **70-10-1**, with the concomitant disappearance of the second re-oxidation peak, was only achieved at a scan rate of 500 V s^{-1} (see also ESI Fig. S1† for CV curves measured at different scan rates; we consider the reduction to be electrochemically reversible when the reduction and re-oxidation currents for the peaks at −0.11 V and −0.05 V become equal and the peak at +0.70 V disappears). These results indicate that at low scan speeds the **70-10-1**$^-$ radical anion is transformed into a new chemical species, the electrochemical oxidation of which corresponds to the anodic peak at *ca.* 0.70 V *vs.* $C_{70}^{0/-}$ (*i.e.*, at low scan speeds the reduction of **70-10-1** is consistent with an electrochemical/chemical (EC) process). Note that the second reduction peak of **70-10-1** peak at −0.66 V is reversible even at low scan rates, and therefore the two consecutive reductions of **70-10-1** are reversible at 500 V s^{-1}.

ESR- and vis-NIR spectroelectrochemistry

The EC reduction process at slow scan rates was investigated using a combination of ESR-SEC and vis-NIR-SEC. Fig. 3 shows that the reduction of **70-10-1** is accompanied by the appearance of several absorption features at wavelengths up to 1200 nm (note that **70-10-1** does not absorb light with λ >

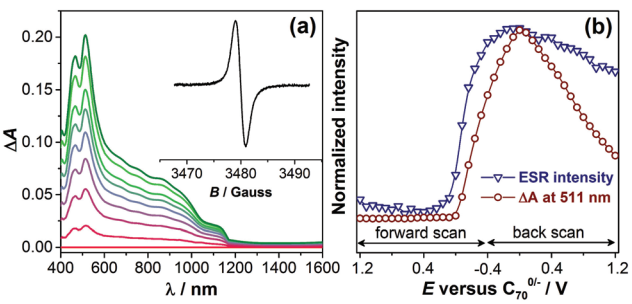

Fig. 3 Vis-NIR/ESR spectroelectrochemical studies of **70-10-1**: (a) difference vis-NIR absorption spectra detected during the first reduction (red zero line corresponds to the potential 1.2 V, green line was measured at −0.4 V); the inset shows the ESR spectrum of the reduced form (g = 2.0031, peak width 2.0 G); (b) evolution of the ESR intensity (double integral) and relative absorbance at 511 nm during cyclic voltammetry at the first reduction step.

520 nm [48]). The formation of a paramagnetic species with a featureless ESR signal was also observed when the potential of the working electrode was more negative than −0.1 V *vs.* $C_{70}^{0/-}$. Qualitatively, the appearance of an ESR signal during the first reduction indicates the formation of a relatively stable radical anion. This could be (**70-10-1**)$^-$ or a paramagnetic species derived from it. In the case of a reversible single-electron reduction, the number of electrons transferred will equal the number of unpaired spins observed. The former can be calculated by integration of the current-*versus*-time dependence, and the latter can be determined from the intensity of the ESR signal. For the SEC experiments shown in Fig. 3, only one unpaired spin was observed for every 12 electrons transferred (see also ESI Fig. S2†). This means that only a small portion of the reduced **70-10-1** is ESR active, whereas the main product of the reduction is ESR silent and likely diamagnetic. Our working hypothesis after performing the ESR-SEC experiment was that the ESR-active (**70-10-1**)$^-$ radical anion is in equilibrium with the putative diamagnetic product, and the distribution of the original **70-10-1** molecules was *ca.* 8% (**70-10-1**)$^-$ and *ca.* 92% diamagnetic product.

ESR spectroscopy can only detect paramagnetic species, but both paramagnetic and diamagnetic compounds can give rise to vis-NIR absorptions. Therefore, the difference absorption spectra in Fig. 3 are largely due to the predominant diamagnetic product. To clarify this point we compared the evolution of the ESR signal intensity and the intense absorption feature at 511 nm during the voltammetric cycle. The two intensity *vs.* potential profiles are different, indicating that these spectral features correspond to different chemical species.

^{19}F NMR spectroscopy and spectroelectrochemistry

We used ^{19}F NMR-SEC to characterize the predominant diamagnetic product formed by one-electron reduction of **70-10-1**. The results are shown in Fig. 4 and 5. The CF_3 groups in **70-10-1** are positioned on a ribbon of edge-sharing *para*- and *meta*-$C_6(CF_3)_2$ hexagons (Fig. 1), and through-space Fermi-contact F···F interactions between CF_3 groups sharing the same hexagon result in ^{19}F NMR quartets for the two CF_3 groups at the ends of the ribbon (these are quartets **i** and **j** in Fig. 5) and quartets of quartets (sometimes appearing as apparent septets or more complex multiplets) for the other eight CF_3 groups (see Table 1 for chemical shifts).[41,49]

Fig. 4 shows the evolution of the ^{19}F NMR spectra recorded *in situ* during the bulk electrolytic reduction of **70-10-1** in *o*-DCB-d_4 at −0.3 V *vs.* $C_{70}^{0/-}$ and re-oxidation of the solution at 1.1 V (the electrolysis times at the two potentials were 6 and 10 h, respectively). As the electrolytic reduction proceeded, the 10 multiplets due to **70-10-1** broadened and decreased in intensity and a new set of 10 multiplets with slightly smaller integrated intensities appeared (*vide supra*). A small amount of **70-10-1** was still present after the bulk electrolytic reduction. Re-oxidation of the sample restored the spectrum of **70-10-1**. No additional spectral features were detected during or after the electrolysis. The lack of NMR signals due to species other than **70-10-1** after electrolysis demonstrated conclusively that

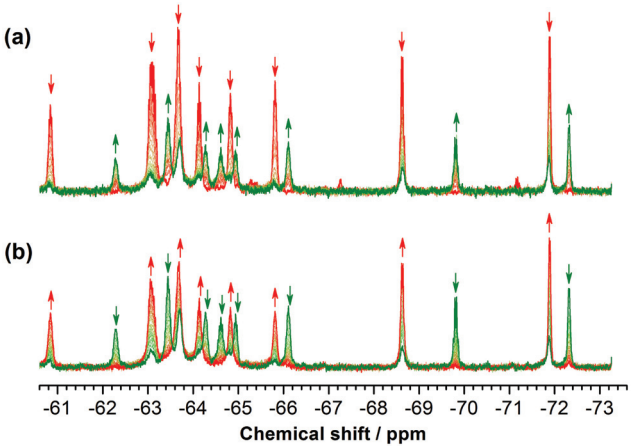

Fig. 4 ^{19}F NMR spectra recorded *in situ* during the bulk electrolysis of **70-10-1** in *o*-DCB-d_4: (a) reduction at −0.3 V *vs.* $C_{70}^{0/-}$; (b) re-oxidation of the solution at +1.1 V. The green spectra in both (a) and (b) correspond to the solution of **70-10-1** after electrolytic reduction. The red spectra in (a) and (b) correspond to the solution of **70-10-1** before the electrolytic reduction and after the electrolytic re-oxidation, respectively. The arrows indicate the increase (up) or decrease (down) in intensity of the indicated multiplets during the electrolytic reduction (a) and the electrolytic re-oxidation (b). The green spectra are assigned to the predominant diamagnetic species formed by the spontaneous transformation of the paramagnetic (**70-10-1**)$^-$ radical anion.

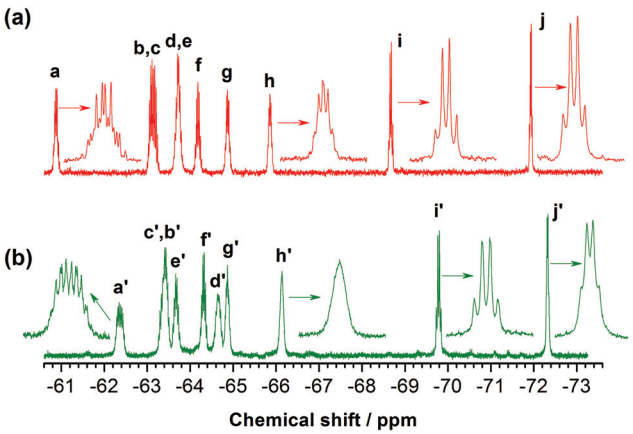

Fig. 5 ^{19}F NMR spectra in *o*-DCB-d_4 of samples of **70-10-1** before (a) and after (b) the addition of excess $Co(Cp)_2$. The assignment of multiplets **a**, **b**, ..., **j** and **a′**, **b′**, ... **j′** to particular CF_3 groups was established using 2D COSY ^{19}F NMR spectra, which are shown in ESI Fig. S4 and S5.† The assignments to particular CF_3 groups are shown in Fig. 1.

the one-electron reduction of **70-10-1** is chemically reversible, even though it is electrochemically irreversible at all but the fastest scan speeds.

A modest excess of the strong one-electron reductant $Co(Cp)_2$ was used to achieve the complete conversion of **70-10-1** to the reduced products, as shown in Fig. 5. The resulting (green) NMR spectrum in Fig. 5 is identical to the green spectra in Fig. 4 and is therefore assigned to the diamagnetic

Table 1 ^{19}F NMR data for **70-10-1** in pristine and reduced forms measured in *o*-DCB-d_4

Compound		Multiplet/−δ/COSY multiplet correlations/J_{FF}, Hz									
70-10-1		**a**	**b**	**c**	**d**	**e**	**f**	**g**	**h**	**i**	**j**
	−δ	60.9	63.1	63.2	63.7	63.8	64.2	64.9	65.9	68.7	71.9
	COSY	**c,g**	**e,f**	**a,h**	**e,i**	**b,d**	**b,g**	**a,f**	**c,j**	**d**	**h**
	J_{FF}, Hz	11,16	13–14	14–16	14–16	13–14	13–16	11,16	10,14	16	10
(**70-10-1**)$_2^{2-}$		**a′**	**b′**	**c′**	**d′**	**e′**	**f′**	**g′**	**h′**	**i′**	**j′**
	−δ	62.4	63.5	63.4	64.7	63.7	64.3	64.9	66.2	69.8	72.4
	COSY	**c′,g′**	**a′,h′**	**e′,f′**	**b′,d′**	**b′,g′**	**e′,i′**	**a′,f′**	**c′,j′**	**d′**	**h′**
	J_{FF}, Hz	13–15	10–13	12–16	14–17	14–16	14–16	10–16	5	17	10

product formed by one-electron reduction of **70-10-1**. 2D COSY experiments (ESI Fig. S3 and S4†) confirmed that the CF_3 addition pattern is a ribbon of *p*- and *m*-$C_6(CF_3)_2$ hexagons. Furthermore, it appears that the multiplets labelled **a′**, **b′**, **c′**, *etc*. in the green spectrum are associated with the same CF_3 groups that give rise to multiplets **a**, **b**, **c**, *etc*. in the spectrum of **70-10-1**. That is, the green and red spectra appear to be congruent except that the multiplets in the green spectrum are shifted to more negative δ values. The largest shifts are for green multiplets **a′** and **i′** (−1.5 and −1.1 ppm relative to red multiplets **a** and **i**, respectively; see Table 1 for additional information). Significantly, the through-space Fermi-contact J_{FF} coupling constants for quartets **i** and **i′** and for **j** and **j′** are similar. Taken together, these results suggest that the positions of the CF_3 groups on the C_{70} cage do not change upon reduction.

After reduction, the integrated intensities of multiplets **a′**, **h′**, **i′**, and **j′** were reduced to 89 ± 3% of the original intensities of multiplets **a**, **h**, **i**, and **j** (these are the multiplets for which the most precise integrated intensities could be measured). This value agrees reasonably well with the ESR-SEC measurements (*i.e.*, *ca.* 10% paramagnetic, "NMR-silent" (**70-10-1**)$^-$ and *ca.* 90% of a diamagnetic, ESR-silent species that exhibits the green ^{19}F NMR spectrum).

Interestingly, the spectral changes induced by the reduction of **70-10-1** are very similar to those observed upon addition of CN^- to **70-10-1**,[50] as shown in Fig. 6. Reaction of **70-10-1** with CN^- gives a monoadduct anion (**70-10-1**)$(CN)^-$ with CN bonded to the C34 atom located on the pole of the fullerene cage.

To summarize, the combined spectroelectrochemical studies of the **70-10-1** reduction mechanism show that (a) the process is chemically reversible (**70-10-1** is fully recovered after re-oxidation); (b) the first reduction produces both diamagnetic and paramagnetic species in a *ca.* 9 : 1 ratio based on the C_{70} cages; (c) the diamagnetic reduction product has a CF_3 addition pattern similar to that of **70-10-1**; (d) the NMR spectrum of one-electron reduced **70-10-1** resembles that of the (**70-10-1**)$(CN)^-$ anion. Based on these results, we propose that (**70-10-1**)$^-$ undergoes spontaneous dimerization to a diamagnetic dianion (**70-10-1**)$_2^{2-}$ held together with a C–C single bond between identical cage C(sp^3) atoms (as **70-10-1** has C_1 symmetry, co-existence of R–S and S–S forms of the dimer and their enantiomers S–R and S–S is probable, but cannot be distinguished in our ^{19}F NMR spectra). Furthermore, we propose that the cage C(sp^3) atom on each **70-10-1** moiety of the (**70-10-1**)$_2^{2-}$ dimer is C34, the same cage C atom that is bonded to the CN group in (**70-10-1**)$(CN)^-$ (hence the similarity of their NMR spectra). Presumably, the diamagnetic dimeric dianion (**70-10-1**)$_2^{2-}$ undergoes two-electron oxidation at *ca.* 0.7 V *vs.* $C_{70}^{0/-}$ to reform **70-10-1**. Hence, **70-10-1** is reformed at the end of the voltammetric cycles shown in Fig. 2.

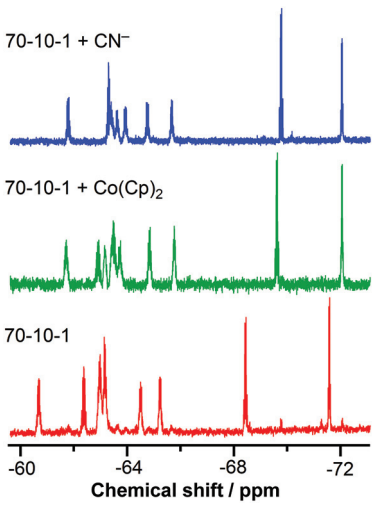

Fig. 6 ^{19}F NMR spectra in CD_2Cl_2 of **70-10-1**, **70-10-1** reduced with $Co(Cp)_2$, and **70-10-1** reacted with CN^-. Note that the chemical shifts are somewhat different from those measured in *o*-DCB.

Mass-spectral studies

In dianionic fullerene dimers, the monomer units experience strong Coulomb repulsion (*e.g.*, in ref. 51, the repulsion energy in fullerene dimer dianions was estimated to be *ca.* 100 kJ mol^{-1}), and hence they are not stable in the gas phase and are not readily detected by mass spectrometry. Nevertheless, we observed a monoanion with twice the mass of **70-10-1** in the NI-APCI mass spectrum of a CH_2Cl_2 solution of a mixture of **70-10-1** and $Co(Cp)_2$ (see ESI Fig. S6†). The dimer and monomer anions were easily oxidized during the analysis by traces of air from the acetonitrile mobile phase. The NI-APCI mass spectrum of **70-10-1** under similar conditions did not exhibit dimeric or oxidized species.

DFT calculations

To clarify the possible molecular structure of the diamagnetic dianionic dimer, we performed a computational study. The most thermodynamically preferable dimerization sites were predicted using the algorithm described previously for anionic fullerene dimers.[51] We first computed the 31 (**70-10-1**)$(CH_3)^-$ anions to find which cage C atoms are the most likely to form a stable fullerene–fullerene C(sp^3)–C(sp^3) single bond (ESI Table S1;† only 31 out of 60 C-sp^2 atoms of **70-10-1** were considered as possible dimerization sites because the other 29 positions are sterically hindered by close CF_3 groups). Using these results as a guide, the 17 most stable $(\mathbf{70\text{-}10\text{-}1})_2^{2-}$ dimers were computed, and these are also listed in Table S2.† The most stable dimeric dianion has a C34–C34 bond (Fig. 7). This is in harmony with the observation that C34 is the **70-10-1** cage C atom that is attacked first by CN^-.[50] All the other calculated $(\mathbf{70\text{-}10\text{-}1})_2^{2-}$ isomers are less stable than the C34–C34 dimer by at least 18 kJ mol^{-1}. Interestingly, C34 is not one of the cage C(sp^2) atoms in $(\mathbf{70\text{-}10\text{-}1})^-$ with high unpaired spin density, as shown in Fig. 7. The atoms with significant unpaired spin density are close to the CF_3 groups and are therefore sterically hindered from forming an intercage C–C bond. Importantly, the C33–C34 bond in **70-10-1** is the most reactive cage C=C double bond and is functionalized first when substituents are added to **70-10-1**.[50,52–54]

Anion radicals of C_{70} are known to dimerize in the solid state,[55] but in solution the monomer is the dominant form, and the electrochemical reduction of C_{70} is reversible even at low scan rates. To explain the difference between anions of C_{70} and **70-10-1**, we computed the binding energies of the $(C_{70})_2^{2-}$ and $(\mathbf{70\text{-}10\text{-}1})_2^{2-}$ dimers (Table 2; a negative value means that the dimer is more stable than the monomer). In the gas phase, the B3LYP//PBE calculations indicate that both dimers are unstable, which is not surprising taking into account the strong Coulomb repulsion. Importantly, however, the dimerization of $(\mathbf{70\text{-}10\text{-}1})^-$ is less endothermic than that of C_{70}^- by 52 kJ mol^{-1}. Since standard DFT functionals underestimate the effect of van der Waals interactions, the values were corrected for dispersion interactions using Grimme's empirical D3 approach.[45] Dispersion interactions stabilize both dimers by *ca.* 60 kJ mol^{-1} but do not change the relative values. The $(\mathbf{70\text{-}10\text{-}1})_2^{2-}$ dimer is still unstable in the gas phase, but only by 9.8 kJ mol^{-1}. C-PCM calculations of the solvation energy in *o*-DCB show that both dimers are strongly stabilized by a polarizable continuum. With $\Delta\Delta E_{solv}$ values of −114 and −97 kJ mol^{-1} for $(C_{70})_2^{2-}$ and $(\mathbf{70\text{-}10\text{-}1})_2^{2-}$, respectively, the dimerizations of C_{70}^- and $(\mathbf{70\text{-}10\text{-}1})^-$ in *o*-DCB are both predicted to be exothermic. In solution, the $(\mathbf{70\text{-}10\text{-}1})_2^{2-}$ dimer is more stable than the $(C_{70})_2^{2-}$ dimer, relative to their respective monomeric monoanions, by 38 kJ mol^{-1}. The enhanced stability of the former thus explains why C_{70} and **70-10-1** have different reduction behaviours. Finally, we note that the enhanced stability of dianionic dimers was previously predicted for some endohedral fullerenes, some of which also exhibit electrochemically irreversible reductions.[51]

Table 2 Binding energies of the $(C_{70})_2^{2-}$ and $(\mathbf{70\text{-}10\text{-}1})_2^{2-}$ dimeric dianions[a]

	DFT, gas	DFT-D3, gas	DFT-D3, *o*-DCB
$(C_{70})_2^{2-}$	120.9	64.2	−49.5
$(\mathbf{70\text{-}10\text{-}1})_2^{2-}$	68.9	9.8	−87.1

[a] Single point energy B3LYP-D3/6-311G* calculations with PBE-optimized structures. All values are in kJ per mol of dimeric anion.

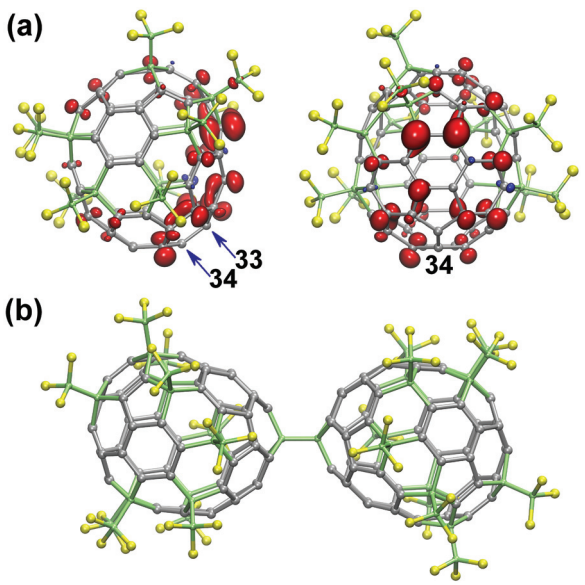

Fig. 7 (a) Spin density distribution in the $(\mathbf{70\text{-}10\text{-}1})^-$ radical anion; two projections of the molecule are shown, and the proposed dimerization sites C34 and C33 are indicated by arrows. (b) The DFT-optimized molecular structure of the most stable $(\mathbf{70\text{-}10\text{-}1})_2^{2-}$ dimer linked through C34.

Conclusions

The redox behaviour of **70-10-1** was studied by a combination of spectroelectrochemical (SEC) techniques, which detected both paramagnetic and diamagnetic species, the latter formed by a chemically reversible EC process. We showed that the $\mathbf{70\text{-}10\text{-}1}^-$ radical anion exists in equilibrium with its singly-bonded diamagnetic dimeric dianion, $(\mathbf{70\text{-}10\text{-}1})_2^{2-}$, in *o*-DCB solution. ^{19}F NMR spectroelectrochemical data are reported here for the first time, and ^{19}F NMR-SEC was shown to be a convenient and useful tool for studying the redox reactions of fluorinated organic compounds. This study also emphasizes the importance of not only qualitative, but also quantitative SEC studies for the reliable elucidation of the redox processes and products of follow-up reactions. Qualitative ESR-SEC study of **70-10-1** reduction detected the formation of the radical anion, but failed to reveal that the main component is ESR silent, which became possible only after a quantitative ESR

study and comparison to the number of transferred charges determined from the voltammogram. Likewise, correspondence of the quantitative ESR and NMR data on the fraction of the reduced form being ESR- and NMR-visible proves that all the electrochemically produced species were identified. Thus, the combination of SEC methods was crucial for the complete description of the redox process.

Acknowledgements

We thank Ulrike Nitzsche for help with the local computational resources in IFW Dresden. Research Computing Center of Moscow State University[56] and The Center for Information Services and High Performance Computing of Technical University of Dresden are acknowledged for computing time. Financial support by DFG (projects PO 1602/1-2 to AAP), and by TU Graz, Stiftung ProBono and MPG to MZ, is highly appreciated. OVB and SHS acknowledge the U.S. National Science Foundation (grant CHE 1362302) and the Colorado State University Foundation for financial support. AAP acknowledges funding from the European Research Council (ERC) under the European Union's Horizon 2020 research and innovation programme (grant agreement No. 648295 "GraM3").

Notes and references

1 J. E. Anthony, A. Facchetti, M. Heeney, S. R. Marder and X. Zhan, *Adv. Mater.*, 2010, **22**, 3876–3892.
2 X. Gao and Y. Hu, *J. Mater. Chem. C*, 2014, **2**, 3099–3117.
3 C. Wang, H. Dong, W. Hu, Y. Liu and D. Zhu, *Chem. Rev.*, 2012, **112**, 2208–2267.
4 C. R. Newman, C. D. Frisbie, D. A. da Silva Filho, J.-L. Brédas, P. C. Ewbank and K. R. Mann, *Chem. Mater.*, 2004, **16**, 4436–4451.
5 M. Mas-Torrent and C. Rovira, *Chem. Soc. Rev.*, 2008, **37**, 827–838.
6 I. V. Kuvychko, K. P. Castro, S. H. M. Deng, X.-B. Wang, S. H. Strauss and O. V. Boltalina, *Angew. Chem., Int. Ed.*, 2013, **52**, 4871–4874.
7 I. V. Kuvychko, C. Dubceac, S. H. M. Deng, X.-B. Wang, A. A. Granovsky, A. A. Popov, M. A. Petrukhina, S. H. Strauss and O. V. Boltalina, *Angew. Chem., Int. Ed.*, 2013, **52**, 7505–7508.
8 I. V. Kuvychko, S. N. Spisak, Y.-S. Chen, A. A. Popov, M. A. Petrukhina, S. H. Strauss and O. V. Boltalina, *Angew. Chem., Int. Ed.*, 2012, **51**, 4939–4942.
9 T. T. Clikeman, E. V. Bukovsky, I. V. Kuvychko, L. K. San, S. H. M. Deng, X.-B. Wang, Y.-S. Chen, S. H. Strauss and O. V. Boltalina, *Chem. Commun.*, 2014, **50**, 6263–6266.
10 L. K. San, E. V. Bukovsky, I. V. Kuvychko, A. A. Popov, S. H. Strauss and O. V. Boltalina, *Chem. – Eur. J.*, 2014, **20**, 4373–4379.
11 B. M. Schmidt, B. Topolinski, M. Yamada, S. Higashibayashi, M. Shionoya, H. Sakurai and D. Lentz, *Chem. – Eur. J.*, 2013, **19**, 13872–13880.
12 B. M. Schmidt, B. Topolinski, S. Higashibayashi, T. Kojima, M. Kawano, D. Lentz and H. Sakurai, *Chem. – Eur. J.*, 2013, **19**, 3282–3286.
13 B. M. Schmidt, S. Seki, B. Topolinski, K. Ohkubo, S. Fukuzumi, H. Sakurai and D. Lentz, *Angew. Chem., Int. Ed.*, 2012, **51**, 11385–11388.
14 L. K. San, T. T. Clikeman, C. Dubceac, A. A. Popov, Y.-S. Chen, M. A. Petrukhina, S. H. Strauss and O. V. Boltalina, *Chem. – Eur. J.*, 2015, **21**, 9488–9492.
15 O. V. Boltalina, A. A. Popov, I. V. Kuvychko, N. B. Shustova and S. H. Strauss, *Chem. Rev.*, 2015, **115**, 1051–1105.
16 R. Taylor, *Chem. – Eur. J.*, 2001, **7**, 4074–4083.
17 O. V. Boltalina and S. H. Strauss, in *Dekker Encyclopedia of Nanoscience and Nanotechnology*, Taylor & Francis, 2nd edn, 2009, pp. 1307–1321.
18 A. A. Popov, I. E. Kareev, N. B. Shustova, E. B. Stukalin, S. F. Lebedkin, K. Seppelt, S. H. Strauss, O. V. Boltalina and L. Dunsch, *J. Am. Chem. Soc.*, 2007, **129**, 11551–11568.
19 A. A. Popov, I. E. Kareev, N. B. Shustova, S. F. Lebedkin, S. H. Strauss, O. V. Boltalina and L. Dunsch, *Chem. – Eur. J.*, 2008, **14**, 107–121.
20 L. Dunsch, *J. Solid State Electrochem.*, 2011, **15**, 1631–1646.
21 W. Kaim and J. Fiedler, *Chem. Soc. Rev.*, 2009, **38**, 3373–3382.
22 S. Klod and L. Dunsch, *Magn. Reson. Chem.*, 2011, **49**, 725–729.
23 S. Klod, F. Ziegs and L. Dunsch, *Anal. Chem.*, 2009, **81**, 10262–10267.
24 S. Klod, K. Haubner, E. Jahne and L. Dunsch, *Chem. Sci.*, 2010, **1**, 743–750.
25 P. Rapta, K. Haubner, P. Machata, V. Lukeš, M. Rosenkranz, S. Schiemenz, S. Klod, H. Kivelä, C. Kvarnström, H. Hartmann and L. Dunsch, *Electrochim. Acta*, 2013, **110**, 670–680.
26 R. Boisseau, U. Bussy, P. Giraudeau and M. Boujtita, *Anal. Chem.*, 2015, **87**, 372–375.
27 U. Bussy, P. Giraudeau, V. Silvestre, T. Jaunet-Lahary, V. Ferchaud-Roucher, M. Krempf, S. Akoka, I. Tea and M. Boujtita, *Anal. Bioanal. Chem.*, 2013, **405**, 5817–5824.
28 U. Bussy, P. Giraudeau, I. Tea and M. Boujtita, *Talanta*, 2013, **116**, 554–558.
29 X. Zhang and J. W. Zwanziger, *J. Magn. Reson.*, 2011, **208**, 136–147.
30 P. D. Prenzler, R. Bramley, S. R. Downing and G. A. Heath, *Electrochem. Commun.*, 2000, **2**, 516–521.
31 J. A. Richards and D. H. Evans, *Anal. Chem.*, 1975, **47**, 964–966.
32 L. M. S. Nunes, T. B. Moraes, L. L. Barbosa, L. H. Mazo and L. A. Colnago, *Anal. Chim. Acta*, 2014, **850**, 1–5.
33 K. Albert, E.-L. Dreher, H. Straub and A. Rieker, *Magn. Reson. Chem.*, 1987, **25**, 919–922.
34 D. W. Mincey, M. J. Popovich, P. J. Faustino, M. M. Hurst and J. A. Caruso, *Anal. Chem.*, 1990, **62**, 1197–1200.

35 R. D. Webster, *Anal. Chem.*, 2004, **76**, 1603–1610.
36 U. Bussy and M. Boujtita, *Talanta*, 2015, **136**, 155–160.
37 A. A. Popov, I. E. Kareev, N. B. Shustova, S. H. Strauss, O. V. Boltalina and L. Dunsch, *J. Am. Chem. Soc.*, 2010, **132**, 11709–11721.
38 A. A. Popov, N. B. Shustova, O. V. Boltalina, S. H. Strauss and L. Dunsch, *ChemPhysChem*, 2008, **9**, 431–438.
39 A. A. Popov, J. Tarabek, I. E. Kareev, S. F. Lebedkin, S. H. Strauss, O. V. Boltalina and L. Dunsch, *J. Phys. Chem. A*, 2005, **109**, 9709–9711.
40 D. V. Konarev, N. A. Romanova, R. A. Panin, A. A. Goryunkov, S. I. Troyanov and R. N. Lyubovskaya, *Chem. – Eur. J.*, 2014, **20**, 5380–5387.
41 I. E. Kareev, I. V. Kuvychko, A. A. Popov, S. F. Lebedkin, S. M. Miller, O. P. Anderson, S. H. Strauss and O. V. Boltalina, *Angew. Chem., Int. Ed.*, 2005, **44**, 7984–7987.
42 A. Petr, L. Dunsch and A. Neudeck, *J. Electroanal. Chem.*, 1996, **412**, 153–158.
43 D. N. Laikov and Y. A. Ustynuk, *Russ. Chem. Bull.*, 2005, **54**, 820–826.
44 D. N. Laikov, *Chem. Phys. Lett.*, 1997, **281**, 151–156.
45 S. Grimme, J. Antony, S. Ehrlich and H. Krieg, *J. Chem. Phys.*, 2010, **132**, 154104.
46 M. Cossi, N. Rega, G. Scalmani and V. Barone, *J. Comput. Chem.*, 2003, **24**, 669–681.
47 A. A. Granovsky, *Firefly, version 8.00*, 2013.
48 K. P. Castro, Y. Jin, J. J. Rack, S. H. Strauss, O. V. Boltalina and A. A. Popov, *J. Phys. Chem. Lett.*, 2013, **4**, 2500–2507.
49 I. E. Kareev, I. V. Kuvychko, S. F. Lebedkin, S. M. Miller, O. P. Anderson, K. Seppelt, S. H. Strauss and O. V. Boltalina, *J. Am. Chem. Soc.*, 2005, **127**, 8362–8375.
50 T. T. Clikeman, I. V. Kuvychko, N. B. Shustova, Y.-S. Chen, A. A. Popov, O. V. Boltalina and S. H. Strauss, *Chem. – Eur. J.*, 2013, **19**, 5070–5080.
51 A. A. Popov, S. M. Avdoshenko, G. Cuniberti and L. Dunsch, *J. Phys. Chem. Lett.*, 2011, 1592–1600.
52 T. T. Clikeman, S. H. M. Deng, A. A. Popov, X.-B. Wang, S. H. Strauss and O. V. Boltalina, *Phys. Chem. Chem. Phys.*, 2015, **17**, 551–556.
53 Y. Takano, M. A. Herranz, I. E. Kareev, S. H. Strauss, O. V. Boltalina, T. Akasaka and N. Martin, *J. Org. Chem.*, 2009, **74**, 6902–6905.
54 N. S. Ovchinnikova, D. V. Ignat'eva, N. B. Tamm, S. M. Avdoshenko, A. A. Goryunkov, I. N. Ioffe, V. Y. Markov, S. I. Troyanov, L. N. Sidorov, M. A. Yurovskaya and E. Kemnitz, *New J. Chem.*, 2008, **32**, 89–93.
55 D. V. Konarev, S. S. Khasanov, G. Saito, A. Otsuka, Y. Yoshida and R. N. Lyubovskaya, *J. Am. Chem. Soc.*, 2003, **125**, 10074–10083.
56 V. V. Voevodin, S. A. Zhumatiy, S. I. Sobolev, A. S. Antonov, P. A. Bryzgalov, D. A. Nikitenko, K. S. Stefanov and V. V. Voevodin, *Open Syst. J.*, 2012, http://www.osp.ru/os/2012/2007/13017641.